SLAC–PUB–8029
December 1998

Presice Measurement of the Weak Mixing Angle from Leptonic Polarization Asymmetries at the SLD Experiment. *

P. L. Reinertsen
Santa Cruz Institute for Particle Physics
University of California
Santa Cruz
Santa Cruz, CA 95064, USA
E-mail: plasse@scipp.ucsc.edu

Representing

The SLD Collaboration
Stanford Linear Accelerator Center
Stanford University, Stanford, CA 94309

Abstract

This paper presents measurements of the leptonic asymmetries in Z^0 decays measured with the SLD detector at the SLAC Linear Collider. A data sample of approximately 500,000 Z^0 boson decays has been used. These measurements lead to a precise determination of the effective weak mixing angle $\sin^2\theta_w^{\rm eff}$. The combined preliminary result is $\sin^2\theta_w^{\rm eff} = 0.23110 \pm 0.00029$.

Presented at the 5th International Workshop on Tau Physics, Santander, Spain, Sep 14-17 1998.

*Work supported by Department of Energy contract DE–AC03–76SF00515.

Precise Measurement of the Weak Mixing Angle from Leptonic Polarization Asymmetries at the SLD Experiment.

P. L. Reinertsen[a*]

[a]Santa Cruz Institute for Particle Physics, University of California, Santa Cruz, Santa Cruz, CA 95064, The United States

This paper presents measurements of the leptonic asymmetries in Z^0 decays measured with the SLD detector at the SLAC Linear Collider. A data sample of approximately 500,000 Z^0 boson decays has been used. These measurements lead to a precise determination of the effective weak mixing angle $\sin^2\theta_w^{\rm eff}$. The combined preliminary result is $\sin^2\theta_w^{\rm eff} = 0.23110 \pm 0.00029$.

1. Motivation

Searches for new physics beyond the Standard Model (SM) generally take two forms. The direct type of search is to look for new particles (e.g. supersymmetric particles) or to search for new interactions (e.g. proton decay). The indirect type of search involves high precision tests of SM predictions. The measurement of $\sin^2\theta_w^{\rm eff}$ belongs to the latter type of search and is probing the electroweak sector of the SM to 0.1 % precision.

2. The SLC

The Stanford Linear Collider (SLC) [1] provides the SLD experiment with polarized electron beams [2] and unpolarized positron beams for collisions at the Z resonance.

2.1. Electron production

The polarized electron source [3] makes use of a Ti-Sapphire laser in conjunction with a set of optics that produces circular polarized light. The helicity state, left- or right-handed, is determined randomly for each bunch by the voltage applied on the Pockels cell (an active birefringent crystal), see Figure 1. The laser is then focused on a strained-lattice GaAs photocathode for photoemission. Depending on the polarization of the incident light the cathode will get its spin $\frac{1}{2}$ state or its spin - $\frac{1}{2}$ state populated (Figure 2). By putting a strain across the crystal, achieved by a custom grown layer of GaAs on a GaAsP substrate, the degeneracy between the $m = \pm\frac{3}{2}$ and $m = \pm\frac{1}{2}$ $P_{3/2}$ valence levels is broken. By fine tuning the wavelength of the incident light ($\sim$ 860 nm) the effect of the straining can be optimized. Typically, electron polarizations between 70% and 80% were achieved (with 100% possible in principle). Without this strain the maximum electron polarization that would be possible is 50%.

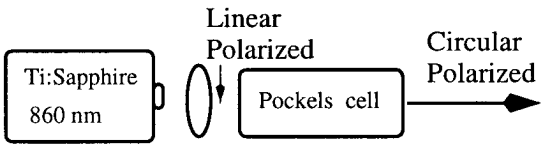

Figure 1. Conceptual description of creating polarized light.

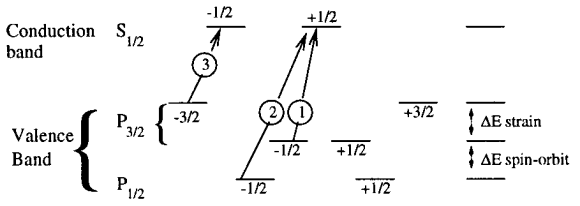

Figure 2. The energy and spin states of the cathode. The relative Clebsch-Gordon coefficients for each transition (for left handed incident light) is indicated on the transition arrows.

*On behalf of the SLD collaboration

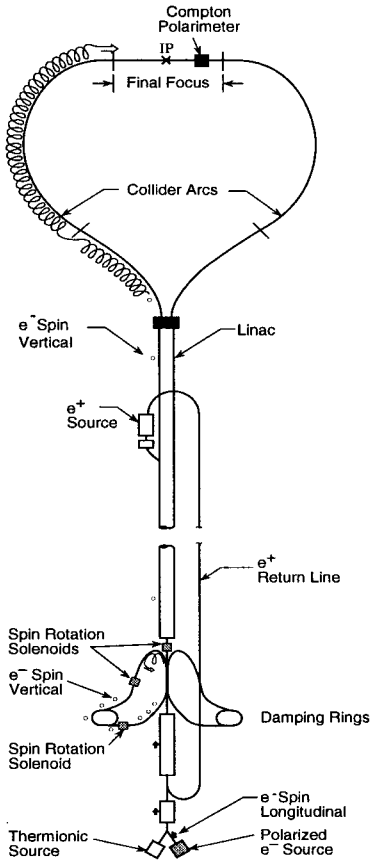

Figure 3. The electron spin transport.

2.2. Transport

The longitudinally polarized electrons are accelerated to the damping ring, where just prior to entering, the polarization is rotated transverse to the plane of the ring. This avoids depolarization in the ring due to finite bunch energy spread (Figure 3). Coming out of the damping ring the electrons are accelerated to full energy at the end of the linac. The energies here are 46.6 GeV for both the electrons and positrons. The electrons and the positrons are then injected into their respective arcs. The electron spin orientation is changed in the arc by controlled vertical trajectory excursions through the existing lattice, which act as a spin rotator system, such as to obtain longitudinal polarization at the SLD IP. The resulting spin transport in the arc is rather complex as indicated by the spiral next to the electron arc. Typically, the electron beam spin vector undergoes an effective 15 rotations in the arc.

2.3. The Polarization Measurement

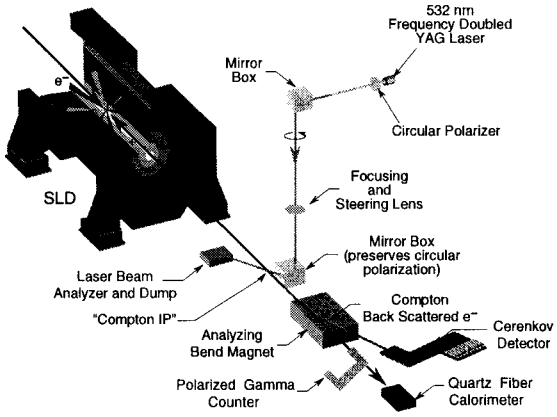

Figure 4. The Compton interaction

After the SLD IP the electrons pass through the Compton IP where circular polarized light is directed head on into the electron bunch to create a Compton interaction (Figure 4). The YAG laser is triggered at approximately every 7th electron beam crossing which gives a rate at around 17Hz.

The Compton backscattered electrons are momentum analyzed by the bending magnet and detected by a transversely segmented Cerenkov detector. The Cerenkov detector is an airtight chamber filled with Propane gas. It consists of nine channels instrumented with phototubes that measure Cerenkov radiation produced by the Compton scattered electrons. The transverse positions of the channels allows for a measurement of the Compton signal as a function of the backscattered electron energy.

The Compton asymmetry A^{Compton} is defined as the asymmetry between the $J = \frac{3}{2}$ spin state (the electron spin and the photon polarization are aligned) and the $J = \frac{1}{2}$ spin state (anti aligned)

$$A^{\text{Compton}} = \frac{N(J=\frac{3}{2}) - N(J=\frac{1}{2})}{N(J=\frac{3}{2}) + N(J=\frac{1}{2})}.$$

Polarization Uncertainty ($\frac{\delta P_e}{P_e} \times 10^2$)

Uncertainty	92	93	94-95	96	1997 (preliminary)	1998 (preliminary)
Laser Polarization	2.0	1.0	0.20	0.20	0.20	0.10
Detector Linearity	1.5	1.0	0.50	0.50	0.50	0.50
Detector Calibration	0.4	0.5	0.29	0.30	0.30	0.30
Electronic Noise	0.4	0.2	0.20	0.20	0.20	0.20
Interchannel Consistency	0.9	0.5	-	-	0.80	0.80
Total Polarimeter Uncertainty	2.7	1.6	0.64	0.64	1.03	1.01
Compton IP $\leftrightarrow$ SLD IP	-	1.1	0.17	0.18	0.07	0.08
Total P_e Uncertainty	2.7	1.9	0.67	0.67	1.03	1.01

Table 1
A detailed list of the systematic uncertainties for the polarization measurement.

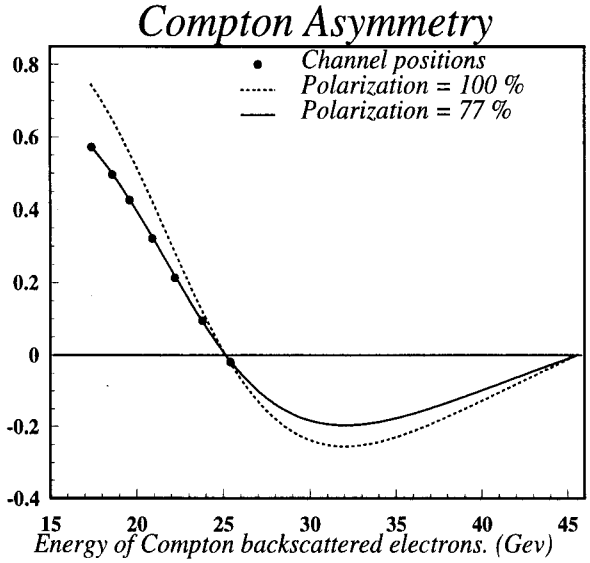

Figure 5. The Compton asymmetry

Figure 5 shows the Compton asymmetry expected if the electron beam were 100% polarized (dashed line) and similarly for 77% electron polarization (solid line). The circular points shows the approximate positions of the seven active Cerenkov channels, the ones within reach of the Compton kinematics between 17 and 45 GeV. The polarization of the electron beam is then found independently by the various channels as the ratio of the measured asymmetry to the expected measurement if the beam were 100% polarized. The process of calculating the expected measured asymmetry for 100% polarized beams, the analyzing power, is described in detail elsewhere [4].

The polarization measurements run parasitically with SLD collisions and one measurement takes three minutes. This corresponds to 3000 Compton interactions and gives a statistical error of around 2%. The continuously measured polarization is plotted in Figure 6 and we see that since 1994 the value has been consistently above 70%.

1992	P_e	=	0.224	$\pm$	0.006	
1993	P_e	=	0.626	$\pm$	0.012	
1994-95	P_e	=	0.772	$\pm$	0.005	
1996	P_e	=	0.765	$\pm$	0.005	
1997	P_e	=	0.733	$\pm$	0.008	Prel.
1998	P_e	=	0.731	$\pm$	0.008	Prel.

Table 2
Luminosity weighted polarization results.

The polarization uncertainties are purely systematic and in Table 1 a detailed list is given for the source of errors. Table 2 shows the luminosity weighted electron polarization averaged for the various SLD runs. Note that the 1997 and 1998 results are preliminary. Errors at the 1996 level or below are expected for the final 1997 and 1998 results.

2.4. Cross checks on the polarization measurements.

While the Cerenkov detector measures the electron beam polarization by detecting the Compton backscattered electrons, two additional detectors

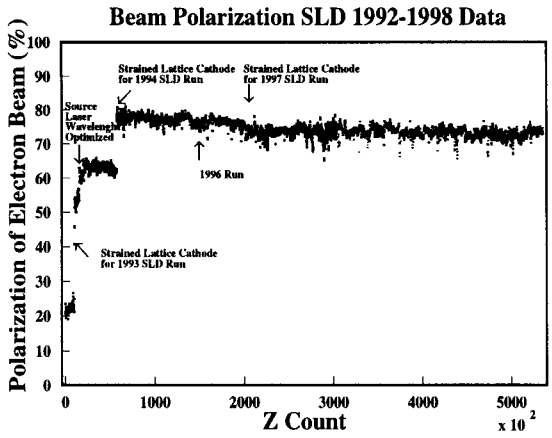

Figure 6. The measured electron polarization as a function of the Z boson count.

measure the electron beam polarization by using the Compton backscattered photons. The Polarized Gamma Counter (PGC) and the Quartz Fiber Calorimeter (QFC) require dedicated one beam (electron only) runs to reduce background and provide sub-1% independent cross checks on the polarization result [5].

3. The SLD

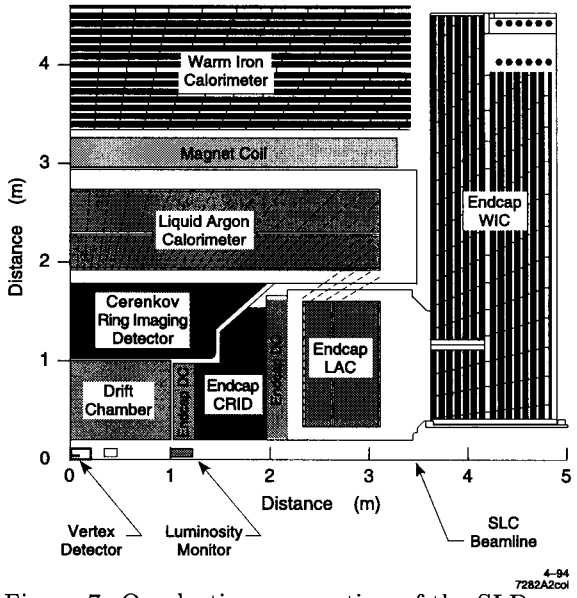

Figure 7. Quadratic cross-section of the SLD.

The $e^+ e^-$ collisions are measured by the SLD detector [6]. It is a general purpose detector which utilizes sub-detectors common for high energy physics (Figure 7). The trigger relies on a combination of calorimeter and tracking information. Event selection is based on the liquid argon calorimeter (LAC) and the central drift chamber tracker (CDC).

The energy resolution for the LAC is

$$\frac{\sigma_E}{E} = \frac{0.15}{\sqrt{E}} \text{ (EM)}, \quad \frac{\sigma_E}{E} = \frac{0.60}{\sqrt{E}} \text{ (HAD)}$$

while for the CDC, the momentum resolution is

$$\frac{\sigma_{p_T}}{p_T} = 0.0095 + 0.0026 p_T$$

4. Theory

In the SM Lagrangian the term that describes the Z boson coupling to fermions is given by

$$\mathcal{L} \propto \bar{\Psi}_f \gamma_\mu (v_f - a_f \gamma_5) \Psi_f Z^\mu,$$

where v_f and a_f denote the strength of the vector and axial vector couplings respectively. The subscript f denotes the particular fermion in question. We can rewrite this piece in the Lagrangian slightly to emphasis the difference between left handed fermions $\Psi_f^L = \frac{1}{2}(1-\gamma_5)\Psi_f$ and right handed fermions $\Psi_f^R = \frac{1}{2}(1+\gamma_5)\Psi_f$

$$\mathcal{L} \propto \bar{\Psi}_f^R \gamma_\mu (v_f + a_f) \Psi_f^L Z^\mu + \bar{\Psi}_f^L \gamma_\mu (v_f - a_f) \Psi_f^R Z^\mu.$$

We see that the nonzero vector axial coupling a_f makes the coupling strength different for left-handed fermions $(v_f + a_f)$ compared to right-handed fermions $(v_f - a_f)$.

The differential polarized cross section for e^+e^- going to a fermion pair through a Z exchange is given by

$$\frac{d\sigma}{dx} \propto (1 - P_e A_e)(1 + x^2) + 2(A_e - P_e) A_f x, \quad (1)$$

where $x = \cos\theta$, with θ being the polar angle with respect to electron beam direction, while A_e and A_f are the initial and final state coupling parameters

$$A_f = \frac{2 v_f a_f}{v_f^2 + a_f^2}, \quad A_e = \frac{2 v_e a_e}{v_e^2 + a_e^2}.$$

A crucial part of this equation is the term dependent on the electron polarization

$$P_e = \frac{N(e_L^-) - N(e_R^-)}{N(e_L^-) + N(e_R^-)}.$$

Here, $N(e_L^-)$ ($N(e_R^-)$) is the number of left-handed (right-handed) electrons in the beam. An illustration of the above formula is shown in Figure 8 for $e^+e^- \to \tau^+\tau^-$. We see that a statistical advantage is afforded from polarization, in form of a large difference between the cross sections of left- and right handed beams.

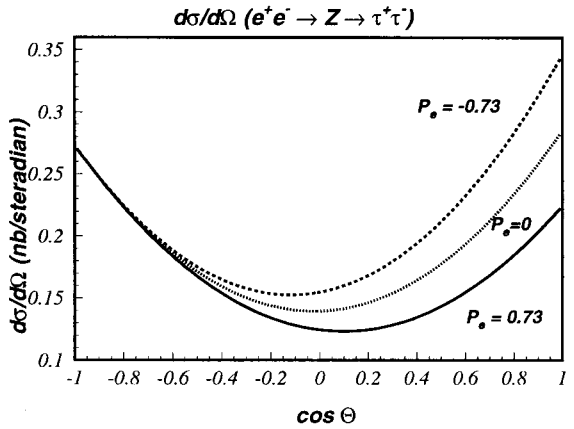

Figure 8. The differential cross-section for $e^+e^- \to Z \to \tau^+\tau^-$.

5. The left-right asymmetry A_{LR}

The measurement of A_{LR} is a straightforward asymmetry between the number of Z bosons produced by left-handed electron beams and the number of Z bosons produced by right-handed electron beams

$$A_{LR}^0 = \frac{\sigma(e_L^- e^+ \to Z) - \sigma(e_R^- e^+ \to Z)}{\sigma(e_L^- e^+ \to Z) + \sigma(e_R^- e^+ \to Z)} \equiv A_e \equiv \frac{2(1 - 4\sin^2\theta_w^{\rm eff})}{1 + (1 - 4\sin^2\theta_w^{\rm eff})^2}, \quad (2)$$

where $\sigma(e_{L(R)}^- e^+ \to Z)$ is found from equation (1) (integrated over $\cos\theta$) with $P_e = 1$ for e_L^- and $P_e = -1$ for e_R^-. Equation (2) also defines the effective mixing angle θ_w with a functional form identical to the tree level expression. Equation (2) incorporates all orders in perturbation theory except for initial state radiation which is by convention kept out. We see that this is a direct measurement of the initial state coupling A_e.

The measured asymmetry A_m is simply a counting experiment

$$A_m = \frac{N_L - N_R}{N_L + N_R}, \quad (3)$$

where N_L and N_R are the number of Z bosons produced by left-handed and right-handed beams respectively. Very small corrections to the measured quantity must be made for background effects and other systematic effects. Let these corrections be denoted by δA_{LR}. Then A_{LR} is defined by

$$A_{LR} = \frac{A_m}{|P_e|} + \delta A_{LR}, \quad \frac{\delta A_{lr}}{A_{LR}} \sim 0.1\%. \quad (4)$$

In addition, a set of corrections needs to be made to the measured quantity A_{LR} in order to turn it into the Z-pole quantity A_{LR}^0. These are the initial state corrections, the $\gamma - Z$ interference terms and the pure γ exchange terms. The total effect of these corrections is around 2% relative, with the interference term being the dominant one. The corrections depend on the energy at which A_{LR} was measured and the actual measured value of A_{LR}.

5.1. Event selection

A_{LR} gets much of its statistical power from the fact that all final states can be used. However, because of complications from t-channel e^+e^- final states the event selection is aimed towards hadronic final states for which wide angle Bhabhas (WAB) are suppressed. As we will see later, the loss of leptonic final states in the A_{LR} analysis are recovered by the polarized forward-backward asymmetry in its contribution to $\sin^2\theta_w^{\rm eff}$.

The event selection requires at least 4 quality tracks (coming from the SLD IP) with an additional requirement that removes e^+e^- final states where one electron radiates a photon that pair produces (one track in one hemisphere and three tracks in the opposite hemisphere). This track multiplicity requirement removes most of the non-hadronic physics events. A minimum energy deposition of 22 GeV is required to remove beam related background and the remaining two-photon events. A last requirement, to reduce non-physics

events, is that of energy balance. The normalized energy vector sum must be less than 0.6.

The above cuts leave the hadronic event selection efficiency at 91-92%. The background in this analysis is small $\mathcal{O}(10^{-3})$ and consists mainly of WAB's.

5.2. Empirical correction to A_{LR}

The empirical correction to A_{LR} ($\delta A_{LR} = \delta A_m/|P_e|$) can be written as

$$\delta A_m = f_b(A_m - A_b) - A_{\mathcal{L}} + A_m^2 A_{\mathcal{P}} - E_{cm}\frac{\sigma'(E_{cm})}{\sigma(E_{cm})}A_E - A_\varepsilon + |P_e|P_P,$$

where f_b is the background fraction and A_b is the left-right asymmetry of this background. $A_{\mathcal{L}}$ is the luminosity asymmetry and $A_{\mathcal{P}}$ is the asymmetry in absolute electron polarization between left- and right-handed beams. P_P is the positron polarization and A_E is the energy asymmetry while A_ε is the detector efficiency asymmetry. The A_ε asymmetry can only be nonzero if the detector tags particles with a different efficiency than antiparticles and if the detector has a significant polar angle acceptance asymmetry. A_ε is assumed to be zero. All other parameters in this expression are constrained by SLD and SLC data. Table 3 gives the preliminary results for the 1996 data. The last three rows are identical to zero.

Asymmetry	Quantity	1996 ($\times 10^{-4}$)
	A_m	1178 ± 44
background	$f_b(A_m - A_b)$	0.65 ± 0.55
luminosity	$A_{\mathcal{L}}$	0.0 ± 0.5
polarization	$A_m^2 A_{\mathcal{P}}$	0.10 ± 0.13
energy	$E_{cm}\frac{\sigma'(E_{cm})}{\sigma(E_{cm})}A_E$	—
Detector ε	A_ε	—
positron polar.	$\lvert P_e\rvert\mathcal{P}_p$	—
	Corr. to A_m	0.76 ± 0.75

Table 3
Systematic corrections to the A_{LR} measurement.

5.3. New cross checks as of 1998

Two important measurements have been performed during the 1998 run. Dedicated run time was provided for both experiments.

The first one is a measurement of the positron polarization [7]. It was measured after the Linac and before the Arc. A foil in a magnetic field provided a polarized electron target for the positrons and the asymmetry in Bhabha scattering, as a function of electron positron spin alignment, was measured [8]. The result verifies zero polarization for the positrons

$$P_P = -0.02\% \pm 0.07\%.$$

The second measurement was a Z-peak scan [9], providing a calibration of the SLD energy spectrometer. It shows that the spectrometer measurements had a small bias and that SLD has been running slightly below the Z-resonance by 40-50 MeV. This corresponds to a relative shift in A_{LR}^0 of $\delta A_{LR}^0/A_{LR}^0 = 0.5\%$. The shift increases A_{LR}^0 slightly moving the SLD result for $\sin^2\theta_w^{\text{eff}}$ lower by about 0.00009.

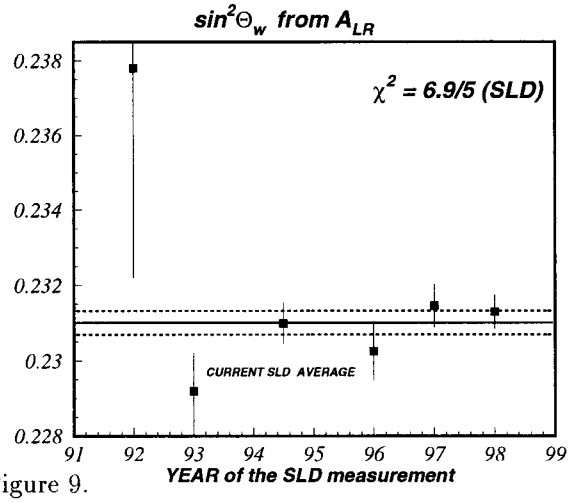

Figure 9.

5.4. The Z-pole results

Table 4 shows the results from the 6 A_{LR} measurements done at the SLD. The first number in each error column is the statistical uncertainty which is the dominant one, the second number is the systematic uncertainty. In Figure 9 the measurements are plotted together with the SLD average. The $\mathcal{X}^2$ for the SLD measurements is 6.9 for 5 degrees of freedom.

6. The left-right forward-backward asymmetries

The left-right forward-backward asymmetry is a double asymmetry which is formed by taking

Run	A^0_{LR}	δA^0_{LR}	$\sin^2\theta^{\rm eff}_w$	$\delta \sin^2\theta^{\rm eff}_w$
1992	0.100	$\pm 0.044 \pm 0.004$	0.2378	$\pm 0.0056 \pm 0.0005$
1993	0.1656	$\pm 0.0071 \pm 0.0028$	0.2292	$\pm 0.0009 \pm 0.0004$
1994-95	0.1512	$\pm 0.0042 \pm 0.0011$	0.23100	$\pm 0.00054 \pm 0.00014$
1996 (preliminary)	0.1570	$\pm 0.0057 \pm 0.0011$	0.23025	$\pm 0.00073 \pm 0.00014$
1997 (preliminary)	0.1475	$\pm 0.0042 \pm 0.0016$	0.23146	$\pm 0.00054 \pm 0.00020$
1998 (preliminary)	0.1487	$\pm 0.0031 \pm 0.0017$	0.23130	$\pm 0.00039 \pm 0.00022$
Combined	0.1510	$\pm$ 0.0025	0.23101	$\pm$ 0.00031

Table 4
The individual measurements from 6 SLD runs.

the difference in the number of forward (F) and backward (B) events for left (L) and right (R) beam polarizations. From equation (1), integrated over forward (and backward) direction, we find

$$\begin{aligned} \tilde{A}^f_{FB} &= \frac{(\sigma_{LF}-\sigma_{LB})-(\sigma_{RF}-\sigma_{RB})}{(\sigma_{LF}+\sigma_{LB})+(\sigma_{RF}+\sigma_{RB})} \\ &= \frac{3}{4}|P_e|A_f, \end{aligned} \quad (5)$$

where for example σ_{LF} is the cross-section for Z's from left-handed beams with a final state particle f (as opposed to an antiparticle) in the forward direction, and similar for the other quantities. The geometrical factor 3/4 (full coverage) depends on detector acceptance and decreases to e.g. 0.6 for $|\cos\theta| < 0.7$. The subscript f denotes the final state particle, which in this paper will be the leptonic ones. We see that this is a direct measurement of the final state parity violating parameters A_f, and for A_μ it is the only existing direct measurement.

The essence of the measurement is contained in equation (5), but instead we perform a maximum likelihood fit, event by event, using the likelihood function L to determine simultaneously A_e and A_μ with μ -pair events (A_e and A_τ with τ-pair events).

$$\begin{aligned} L(A_e, A_f, x, P_e) &= c_z\sigma_z(A_e, A_f, x, P_e) \\ &\quad + c_\gamma\sigma_\gamma(A_e, A_f, x, P_e) \\ &\quad + c_{z\gamma}\sigma_{z\gamma}(A_e, A_f, x, P_e). \end{aligned}$$

Here, σ_Z, σ_γ and $\sigma_{Z\gamma}$ are the tree-level differential cross sections for Z exchange, photon exchange and their interference. The coefficients c are the relative size of the cross sections and take into account initial state radiation. For e^+e^- final states we include the t-channel contribution in the likelihood function. The maximum likelihood fit is less sensitive to detector acceptance as a function of polar angle, and has more statistical power.

6.1. Event selection

The event selection is somewhat more involved for this analysis than for A_{LR}. First, one needs to separate leptonic final states from hadronic final states; secondly, one needs to separate between the various leptonic final states.

A pre-selection requires leptonic-pair events to have between 2 and 8 charged tracks. This excludes most hadronic Z decays, which have an average track multiplicity of around 20. One hemisphere must have a net charge of -1 and the other a net charge of +1 to ensure unambiguous assignment of the scattering angle.

Due to large electromagnetic showering, large energy deposition in the LAC (> 45 GeV) is the only additional requirement to select e^+e^- final states.

$\mu^+\mu^-$ final states are tagged by large invariant mass of the measured tracks, leaving only e^+e^- and $\mu^+\mu^-$, and low energy deposition in the LAC (< 10 GeV for each track), which removes the e^+e^- final states.

The τ selection is the most complicated. It requires that the invariant mass must be less than 70 GeV. The energy deposition in the LAC must be less than 27.5 GeV for each track. At least one stiff track is mandated (> 3 GeV). Further, the acollinearity (the angle between the momenta sums in each hemisphere) must be greater than

160^0. To further suppress hadronic final states, the invariant mass in each hemisphere must be less than 1.8 GeV. Figure 10 shows the angular distribution of the selected events. The points are data and the lines are the best fits. The data is corrected for lower detector efficiency for $|\cos\theta| > 0.7$.

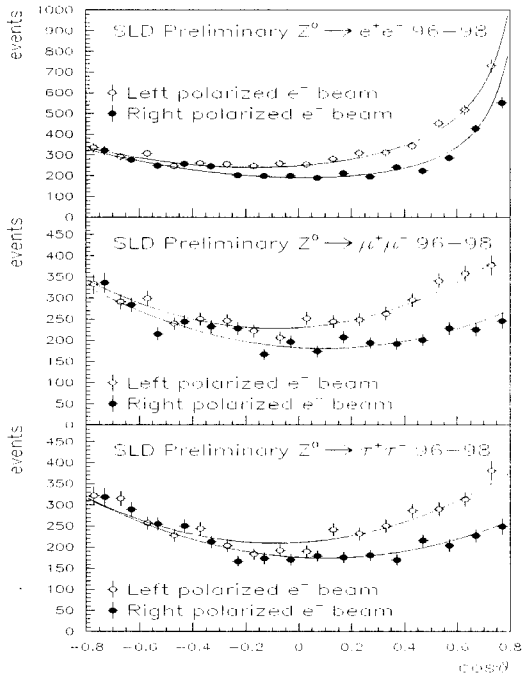

Figure 10. Polar angle distributions for leptonic final states.

6.2. Background corrections

The electron and muon final states have very small backgrounds, the sizes of which have been determined by MC studies. The tau final states have significant background and is studied by using samples of background-rich events selected from the data itself. These events were used to estimate the polar-angle distribution of the background events that eventually populate the tau sample. Table 5 lists the backgrounds and the efficiencies for the 1996-1998 data.

The dominant systematic shift on the A_τ measurement is the V-A effect. As opposed to the other leptonic final states, the taus are only detected through their decay products, and for example, if both taus decay to $\pi\nu$ the helicity of the decaying taus (which is anti correlated in an Z decay) will alter the energy of the tagged π. Both pions will generally be high in energy in the case of a left-handed τ^- and right-handed τ^+ or low in energy otherwise. This effect, which will bias the reconstructed event mass, is large at the SLD because the high beam polarization induces very high and asymmetric tau polarization as a function of the polar angle. The impact of the V-A on the fitted parameter A_τ are listed in Table 6 together with other corrections.

Sample	%	Bckg	ε	events
e^+e^-	1.2%	$\tau^+\tau^-$	87.3%	9419
$\mu^+\mu^-$	0.2%	$\tau^+\tau^-$	85.5%	7564
	0.7%	e^+e^-		
$\tau^+\tau^-$	2%	$\mu^+\mu^-$	78.1%	7088
	1.7%	2γ		
	0.8%	Hadrons		

Table 5
Background and efficiency for $|\cos\theta| < 0.8$

Final State	Bckg.	$\delta A_e(\times 10^4)$	$\delta A_\tau(\times 10^4)$
e^+e^-	$\tau^+\tau^-$	4±4	
$\tau^+\tau^-$	e^+e^-		-2 ± 2
	2 γ	25 ± 25	18 ± 18
	Hadron		13 ± 13
	V-A		-130 ± 29
$\tau^+\tau^-$ total		25 ± 25	-101 ± 37

Table 6
Systematic corrections to A_e and A_τ from tau and electron final states. Corrections to A_μ can be neglected.

6.3. Preliminary results

The leptonic asymmetry measurements are consistent with lepton universality and the individual results, together with the combined result $A_{e,\tau,\mu}$, are listed below

$$A_e = 0.1504 \pm 0.0072$$
$$A_\mu = 0.120 \pm 0.019$$
$$A_\tau = 0.142 \pm 0.019$$
$$A_{e,\mu,\tau} = 0.1459 \pm 0.0063$$

The corresponding value for the weak mixing angle is

$\sin^2\theta_w^{\rm eff} = 0.2317 \pm 0.0008$

7. Combined result

The A_{LR} measurements use hadronic final states and the $\tilde{A}_{FB}^{leptonic}$ uses leptonic final states. Hence, the data sample are complimentary to each other and a combined result for $\sin^2\theta_w^{\rm eff}$ can be made from the measurements of the leptonic parity violating parameters A_l herein. The SLD preliminary running average is

$\sin^2\theta_w^{\rm eff} = 0.23110 \pm 0.00029.$

This result is almost identical to the results from A_{LR} alone and is 2.2 σ different from the global LEP average ($\sin^2\theta_w^{\rm eff} = 0.23187 \pm 0.00024$) is now 2.2 σ. The difference after the 1996 run was almost 3 σ. Added statistics to the SLD result combined with smaller changes from LEP have resulted in better agreement.

It is interesting to note that the LEP leptonic average ($\sin^2\theta_w^{\rm eff} = 0.2315 \pm 0.0004$), from the tau-polarization P_τ and the forward-backward leptonic asymmetries A_{FB}^l, only differs by 0.8 σ from the SLD average.

8. Electroweak measurements, the Higgs mass and/or new physics.

These high precision measurements allow us to not only test the SM but also to probe possible new physics. The SM predictions are calculated from a set of diagrams

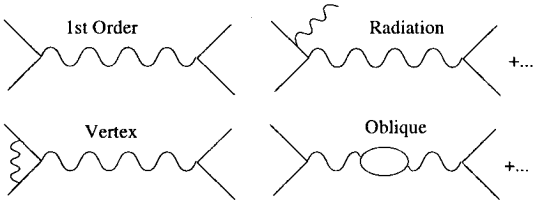

where in particular the oblique diagram will make the SM predictions sensitive to the mass of the Higgs boson (and the top mass). It is expected that new physics will mostly contribute to the oblique type of diagrams [10]. We will now describe a method by Peskin and Takeuchi [10] for parameterizing oblique corrections to neutral currents. In general the oblique diagrams will have the SM particles in the loop in addition to new physics,

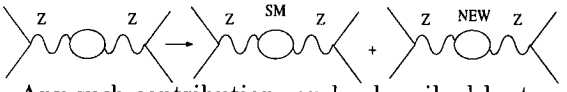

Any such contribution can be described by two parameters S and T,

$$S = S_{SM} + S_{new} \qquad T = T_{SM} + T_{new}$$

The SM predictions uses a preferred value for the top and the Higgs mass. The dependence of the SM on these parameters can then be expressed as

$$S_{SM} = S_{SM}^{ref} + \frac{1}{12\pi}\ln\left[\frac{m_H^2}{m_{H,ref}^2}\right] - \frac{1}{6\pi}\ln\left[\frac{m_t^2}{m_{t,ref}^2}\right]$$

$$T_{SM} = T_{SM}^{ref} - \frac{3}{16\pi c^2}\ln\left[\frac{m_H^2}{m_{H,ref}^2}\right] + \frac{3}{16\pi s^2 c^2}\left[\frac{m_t^2 - m_{t,ref}^2}{m_Z^2}\right]$$

where the tree level parameters $s = \sin\theta_w$ and $c = \cos\theta_w$.

Deviations between measured parameters (effective parameters) and the SM predictions can now be expressed as

$$\sin^2\theta_w^{\rm eff} = \sin^2\theta_w^{ref}\big|_{SM} + \frac{\alpha}{c^2 - s^2}\left[\frac{1}{2}S - s^2c^2T\right],$$

where we have used the Z-pole effective weak mixing angle as an example. Similar expressions exist for other observables such as m_z. For example, if the new physics is a fermion doublet (N,E) with the usual left-handed coupling to $SU(2)$ and masses $M_n, M_E \gg m_Z$ and ($|M_N - M_E| \ll M_N, M_E$) we have

$$S = S_{SM} + \frac{1}{6\pi}$$

$$T = T_{SM} + \frac{1}{12\pi s^2 c^2}\left[\frac{(M_N - M_E)^2}{m_Z^2}\right]$$

Hence, S is viewed as a measure of the total size of the new sector while T is a measure of the total weak isospin breaking induced by it.

Figure 11 shows a S-T plot with various measurements being compared to the SM prediction and a minimal supersymmetric model (MSSM).

The banana shaped region is the SM predictions for $m_t = 173.9 \pm 5.2$ GeV and $M_H \in [88, 1000]$ GeV. The dots are the MSSM prediction for various choices of the 5 MSSM parameters [11]. The straight lines are the measurements with their 68% confidence limit. The elliptical confidence regions (68% and 95%) are a fit to the world's electroweak data. We see that the measurements are in good agreement with the SM predictions and that a light Higgs mass is preferred. No definite conclusions can be made regarding any exclusions of the SM.

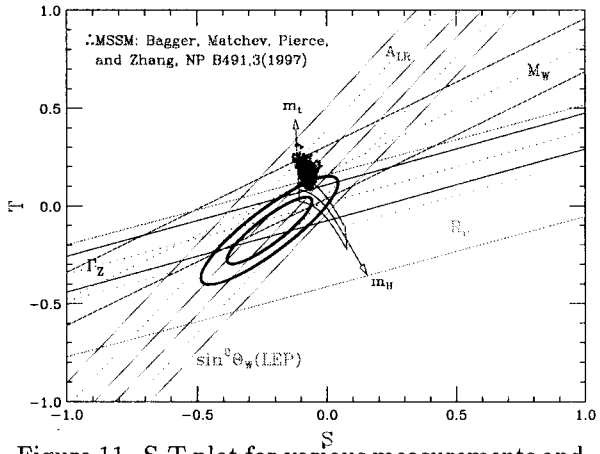

Figure 11. S-T plot for various measurements and predictions.

Figure 12 shows a plot where the SM predicted effective mixing angle is plotted versus the Higgs mass. The dashed curved lines indicate the sensitivity to the top mass. The LEP and the SLD measurements are also indicated on the plot, with the SLD central value being inside the excluded region from direct searches. We see again that both measurements agree well with the SM and that the SLD favors a lighter Higgs mass than the LEP.

9. Conclusion

We have presented the SLD measurement of the weak mixing angle. The leptonic asymmetries are consistent with lepton universality and the combined (preliminary) result is $\sin^2\theta_w^{\rm eff} = 0.23110 \pm 0.00029$, including 1992-1997 data and parts of the 1998 data sample. We expect the

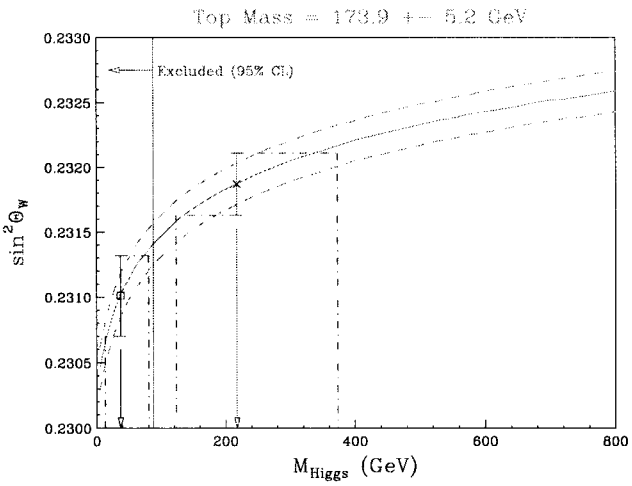

Figure 12. The SLD and the LEP predictions for the Higgs mass assuming that SM is correct.

error to decrease slightly (around 10% relative), partly due to added data, and partly due to lower systematic errors, when the final results are available.

REFERENCES

1. P.Raimondi et al., SLAC-PUB-7955, (1998).
2. M. Woods, SPIN96 Proceedings, 623 (1997).
3. R. Alley et al., Nucl. Inst. Meth. A365, 1 (1995).
4. M. Fero et al., SLD Physics Note 50.
5. R. C. Field et al., OREXP 97-04, (1997); D. Onoprienko et al., UTKHEP 97-20 (1997); D. Onoprienko, SPIN98, conference proceedings.
6. The SLD Design Report, SLAC Report 273, (1984).
7. Private discussions with H. R. Band and P. Rowson.
8. H. R. Band et al., Nucl. Inst. Meth. A400, 24-33 (1997);
9. Private discussions with S. Hertzbach, P. Rowson and M. Woods.
10. M. E. Peskin and T. Takeuchi, Phys. Rev. D46:381-409,(1992).
11. D. M. Pierce, SLAC-PUB-7937, 47pp (1997).